Applied Science and Engineering Progress, Vol. 20, No. 4, 2027, 8320

Research Article

Unravelling the DNA Binding Interactions and Genotoxicity of Cerium Sulfide Nanoparticles

S Farhat Afsar
Department of Biotechnology, M.S. Ramaiah Institute of Technology (affiliated to Visvesvarya Technological University), MSR Nagar, Bangalore - 560054, India

Chandra Prabha M N*
Department of Biotechnology, M.S. Ramaiah Institute of Technology (affiliated to Visvesvarya Technological University), MSR Nagar, Bangalore - 560054, India
Centre for Bio and Energy Materials Innovation, M. S. Ramaiah Institute of Technology, MSRIT Post, Bangalore - 560054, India

D L Monika
Department of Physics, SJB Institute of Technology, Bangalore-560060

R Hari Krishna
Department of Chemistry, M.S. Ramaiah Institute of Technology, MSR Nagar, Bangalore - 560054, India
Centre for Bio and Energy Materials Innovation, M. S. Ramaiah Institute of Technology, MSRIT Post, Bangalore - 560054, India

* Corresponding author. E-mail: chandra@msrit.edu DOI: 10.14416/j.asep.2026.10.001
Received: 21 May 2026; Revised: 20 August 2026; Accepted: 24 August 2026; Published online: 8 October 2026
© 2026 King Mongkut's University of Technology North Bangkok. All Rights Reserved.

Abstract
Metal sulfide nanoparticles (NPs) are extensively explored for biomedical applications, yet their interactions with DNA are essential for evaluating their biological safety. The DNA-binding and genotoxic potential of cerium sulfide NPs (Ce_2S_3 NPs) remain poorly defined. This study evaluates the interaction of solvothermally synthesized Ce_2S_3 NPs with calf thymus DNA (CT-DNA) and their genotoxic effects using complementary spectroscopic, electrochemical, and biological approaches. X-ray diffraction (XRD), Fourier-transform infrared spectroscopy (FTIR), field-emission scanning electron microscopy (FE-SEM), and transmission electron microscopy (TEM) revealed a wurtzite crystal structure with particle sizes of 16 - 40 nm. Surface charge measurements indicated a point of zero charge (pH_pzc) of 6, consistent with protonation under acidic conditions and deprotonation under basic conditions, providing complementary evidence for the electrostatic interaction between DNA and the Ce_2S_3 NPs. UV–visible spectroscopy revealed a hypochromic effect, with a binding constant (K_b) of 5.19×10^4 M^{-1}, indicating moderate DNA-binding affinity. Fluorescence quenching yielded a Stern-Volmer constant (K_{sv}) of 1.57×10^4 M^{-1} and a K_b of 6.71×10^6 M^{-1}, consistent with predominantly through static quenching. Circular dichroism (CD) spectroscopy confirmed retention of the native B-form of CT-DNA, indicating non-intercalative binding. Cyclic voltammetry suggested an electrostatic, with an estimated K_b of 1.70×10^4 M^{-1}. Comet assay revealed dose-dependent DNA damage: limited genotoxicity at lower Ce_2S_3 NPs concentrations, and increased DNA damage at higher concentrations. These findings indicate a concentration-dependent transition from relatively limited DNA interactions at lower concentrations to detectable genotoxic effects at higher concentrations, suggesting the need for dose optimization to ensure their safe and effective use in biomedical applications.

Keywords: Cerium sulfide, Calf thymus DNA, Binding affinity, DNA Binding studies, Genotoxicity

Applied Science and Engineering Progress, Vol. 20, No. 4, 2027, 8320

1 Introduction

Nanoparticles (NPs) have emerged as a promising material in biomedical research because their distinctive nanoscale physicochemical properties, including high, tunable surface area, enhanced reactivity and versatile surface functionalization, make them effective for interactions with biomolecules such as DNA [1]-[3]. The DNA-NP interactions facilitate applications in diagnostics, therapy, biosensing and gene delivery [4]-[6]. Three primary mechanisms explain DNA-NP binding interactions: groove binding [7], and electrostatic interactions [8], and intercalation [9], which are important because they determine nanoparticle stability, cellular uptake, therapeutic efficiency, and potential biological toxicity.

Among inorganic nanomaterials, metal sulfide NPs have attracted increasing interest owing to their favourable optical, electrical, and surface properties, together with good thermal stability [10], [11]. Mahantappa *et al.,* [12] studied the binding interaction of nano zinc sulfide with CT-DNA, the study showed that the ZnS NPs interact primarily via electrostatic attraction and groove binding, accompanied by changes in DNA stability and redox behavior. The metal sulfide reactive surfaces offer controlled release of therapeutic compounds and their antioxidant properties protect DNA against oxidative damage [13], [14].

Cerium based NPs have attracted considerable interest because of their distinctive physicochemical and redox properties. Among these nanomaterials, cerium oxide NPs have been particularly investigated for their reversible Ce^{3+}/Ce^{4+} redox cycling, enabling potent antioxidant and reactive oxygen species scavenging activity. In addition, their oxygen vacancy-rich surface and high catalytic activity facilitate the modulation of redox- sensitive signalling pathways, thereby contributing to anti-inflammatory and cytoprotective effects. Furthermore, the relatively low cytotoxicity and good biocompatibility of cerium-based NPs support their potential use in targeted therapy, bioimaging, drug delivery and neuroprotection [15]-[17].

Spectroscopic investigations show that CeO_2 NPs binding causes hypsochromic shifts and variations in DNA melting temperatures, indicating concentration and surface chemistry dependent impacts on DNA double helix stability [18]. Toxicological studies using *Allium cepa* root cells showed concentration-dependent DNA damage caused by CeO_2 exposure, with comet assay results showing DNA fragmentation in approximately 40% of cells exposed to 100 ppm CeO_2 NPs for 4 h, compared with less than 10% in untreated controls [19].

Although cerium oxide has been extensively investigated for its redox-mediated biological activity, cerium sulfide remains a relatively underexplored nanomaterial for biomedical applications. Compared to CeO_2, Ce_2S_3 combines the redox flexibility of cerium with the more reactive sulfide surface, which may provide distinct electronic characteristics and enhanced surface interactions with biomolecules. The presence of sulfide ions tends to modify the chemical environment of the surface, potentially improving interactions with biomolecules through surface coordination and other non-covalent interactions. Further, the nano size and surface characteristics of Ce_2S_3 NPs may enhance their interactions with cellular components and DNA. Such physicochemical properties are hypothesized to influence oxidative stress and DNA damage in cerium-based nanomaterials. Therefore, Ce_2S_3 NPs are expected to exhibit concentration-dependent genotoxic effects. However, the molecular mechanism and genotoxic potential have not been systematically investigated. This gap motivated the present study, which aims to elucidate the interaction between Ce_2S_3 NPs and calf thymus DNA using spectroscopic and electrochemical methods, along with comet assay-based genotoxicity evaluation. By integrating spectroscopic, electrochemical, and biological approaches, this study aims to elucidate our understanding of Ce_2S_3 NPs-DNA interactions, leading to the design of safer and effective nanomaterials for gene therapy, diagnostics, and other cutting-edge biomedical technologies.

2 Materials and Methods

2.1 *Experimental setup and measurements*

Cerium nitrate hexahydrate ($Ce(NO_3)_3.6H_2O$, purity 99%, SRL Chemicals) was used. Sodium sulphide ($Na_2S.XH_2O$, 99% SDFCL), Thioacetamide (CH_3CSNH_2, purity 98%, Sigma Aldrich), Tris free base ($C_4H_{11}NO_3$, purity 99.9 % HiMedia), absolute Ethanol (C_2H_5OH, Sigma Aldrich) and Calf Thymus DNA (CT-DNA, with highly polymerized, sodium salt, type XI, 42% GC content, Genie Labs Bangalore) were used, Ethidium bromide (Et-Br, $C_{21}H_{20}BrN_3$, Analytical grade, SDFCL), Normal melting agarose (RM 6249-25G, HiMedia), Low melting agarose (RM861-25G, HiMedia), Sodium chloride (NaCl,

purity 99.9% SDFCL), Dulbecco's phosphate-buffered saline (D-PBS, Sigma Aldrich) were purchased, Ficoll-paque plus (GE17-1440-02, Sigma Aldrich), Fetal bovine serum (FBS, Thermo Fisher Scientific) were procured, Roswell Park Memorial Institute (RPMI-1640 medium EDTA, Thermo Fisher Scientific) were commercially obtained, the other chemicals which were used during analysis were of analytical grade reagents.

The stock solution with a known amount of Ce_2S_3 NPs was prepared using Tris-HCl buffer, CT-DNA solution was prepared by dissolving in Tris- HCl buffer and until further use it was stored at 4°C. The concentration of DNA was determined spectrophotometrically by recording absorption measured at 260 nm, using molar absorption coefficient values of 13,200 M^{-1} for double-stranded DNA (dsDNA). Additionally, human genomic DNA was extracted from normal white blood cells (WBCs), which were obtained from peripheral blood.

2.2 *Synthesis of Ce_2S_3 NPs*

Ce_2S_3 NPs were prepared by the solvothermal method in an autoclave with slight modifications from the reported procedure [20]**.** Briefly, 4.34 g of cerium nitrate hexahydrate and 3.756 g of thioacetamide extra pure and 0.254 g of sodium sulphide were dissolved in a mixed solvent containing distilled water and absolute ethanol (Water: Ethanol = 40:60, v/v). The water-ethanol mixture was selected after preliminary optimization, as it provided suitable precursor solubility and promoted controlled nucleation and uniform growth of Ce_2S_3NPs. The mixture was subjected to magnetic stirring to achieve homogeneity and then was transferred to the hydrothermal autoclave maintained at 160 ºC for 16 hours under autogenous (self-generated) pressure in a hot air oven, then cooled at room temperature. The solution was then centrifuged with distilled water and ethanol multiple times. The washed sample was vacuum dried at 70 ºC for 24 hours, resulting in the synthesis of Ce_2S_3NPs. The resulting sample was calcined in an N_2 atmosphere at 300 ^{O}C for 2 hours.

2.3 *Characterization studies*

XRD analysis was carried out to investigate the structural characteristics and crystallographic phase of Ce_2S_3 NPs. Measurements were performed on a Bruker D8 ADVANCE X-ray diffractometer employing Cu Kα radiation (λ = 1.5406 Å). Diffraction patterns were collected over a 2θ range of 10 to 80° with a step size corresponding to a scan rate of 0.5 second per step at ambient temperature.

The functional groups and bonding features of the Ce_2S_3 NPs were analyzed via FT-IR spectroscopy in the 400-4000 cm^{-1} region employing a using a PerkinElmer Spectrum 100 instrument. The particle size, morphology and size distribution of the Ce_2S_3 NPs were further characterized by transmission electron microscopy (TEM) performed on a JEOL JEM-2100 Plus (Japan) operated at an accelerating voltage of 200 kV, providing a point resolution of ~0.2 nm. Selected area electron diffraction (SAED) patterns were measured to evaluate the crystallinity of the NPs. Surface morphology was analysed using FE-SEM carried out on a Carl Zeiss ULTRA 55 (Germany) instrument. The surface charge characteristics were analysed via equilibrium pH measurements by determining the point of zero charge (pH_pzc). DNA concentration was measured using UV-Vis spectrophotometry at 260 nm, with a molar absorption coefficient of 6600 M^{-1} cm^{-1} for double-stranded DNA (dsDNA) [21]. The purity of DNA was evaluated using the A_{260}/A_{280} absorbance ratio, and the values obtained were between 1.8 and 1.9, confirming the purity of the DNA [22].

2.4 *Surface charge of Ce_2S_3 NPs*

A series of eight Erlenmeyer flasks were each filled with 20 mL of 0.01 N NaCl solution. The initial pH of the solution was adjusted between 2 and 9 using 0.01 N HCl or 0.01 N NaOH, following the procedure described in the previous study [23]. After adjusting the pH, 0.01 g of Ce_2S_3 NPs was added to each flask. Immediately sealed flasks were placed in an incubator shaker and operated at 150 rpm at room temperature for 15 hours to allow the system to reach equilibrium. Following equilibration, the pHpzc of Ce_2S_3 NPs was determined from the difference between the final and initial pH values ($\Delta pH = pH_{final} - pH_{initial}$) equals zero [24].

2.5 *DNA binding studies of Ce_2S_3 NPs with CT-DNA*

2.5.1 UV-visible spectroscopy

The DNA- binding behavior of synthesized Ce_2S_3 NPs was investigated using UV-Visible absorption spectroscopy. The absorption spectra were recorded in the 200–600 nm region and the measurements were carried out on an Analytik Jena Specord 210 Plus UV–

Applied Science and Engineering Progress, Vol. 20, No. 4, 2027, 8320

Vis spectrophotometer (Germany). The purity of calf thymus DNA (CT-DNA) was verified by evaluating the absorbance ratio at 260 nm and 280 nm, ensuring its suitability for subsequent binding studies. A known amount of Ce_2S_3 NPs was dispersed in Tris buffer and subjected to sonication for 1.5 h at 50 Hz to obtain a homogeneous suspension. The absorbance was recorded initially at the maximum absorption wavelength (λmax) of 330 nm. For DNA binding studies, CT-DNA was added incrementally (from 25 µL to 400 µL) to a constant volume of the Ce_2S_3 NP solution, and the absorbance was recorded after each addition of CT-DNA. Here, the binding constant (K_b) was calculated from the ratio of the intercept to the slope by plotting a graph of $1/(A-A_0)$ versus $1/C$, where A is the absorbance of the Ce_2S_3 NPs solution and A_0 corresponds to the absorbance of the Ce_2S_3 NPs solution with each 25 µL addition of CT-DNA, following the reported method [25].

2.5.2 Fluorescence spectroscopy

The molecular interaction of Ce_2S_3 NPs with CT-DNA was performed using Fluorescence spectroscopy and was conducted using a Hitachi F-7000 fluorescence spectrofluorometer coupled with a quartz cuvette and a thermostatically controlled cell holder. An ethidium bromide (EtBr), a well-known DNA intercalating dye, was prepared by dissolving 20 mg of EtBr in 2 mL of double-distilled water [12]. The excitation wavelength was fixed at 465 nm, and emission spectra were recorded in the range of 485-800 nm, using 5 nm slit widths for both excitation and emission. Fluorescence quenching experiments were performed by the successive addition of Ce_2S_3 NPs in 50 µM increments to a cuvette containing 30 µM CT-DNA and 20 µM EtBr in Tris buffer (pH 7.4). The fluorescence quenching of DNA-bound EtBr induced by Ce_2S_3 NPs was analyzed using the Stern-Volmer equation, as described in the literature [26].

2.5.3 Circular dichroism

CD spectroscopic analysis was performed to study the changes in the secondary structure of CT-DNA induced by increasing concentrations of Ce_2S_3 NPs. The measurements were conducted using a 1 cm optical path length cuvette, with the CD spectra (JASCO Circular Dichroism Spectrometer) under continuous nitrogen (N_2) purging, recorded in the range of about 220 - 320 nm by performing the background corrections using buffer as a blank [27].

2.5.4 Cyclic voltammetry

An electrochemical workstation (BioLogic SP-150) was used to perform the Cyclic voltammetry (CV). A glassy carbon electrode (GCE) modified with calf thymus DNA (CT-DNA) was employed as the working electrode. Prior to modification, the GCE surface was thoroughly rinsed with deionized water after being polished with an alumina slurry (0.03 µm) on a micro-cloth pad. Following this, the electrode surface was washed with 30% H_2O_2 and 0.1 M HNO_3, and finally rinsed again with deionized water to remove residual impurities. To obtain the DNA-modified electrode, 10 µL of CT-DNA solution was drop-cast on the pre-polished GCE surface and incubated for 24 hours at ambient temperature to promote DNA immobilization and development of a stable modified layer. The electrochemical measurements were performed using a saturated calomel electrode (SCE) as the reference electrode and a platinum wire as the auxiliary (counter) electrode [12]. The electrolyte solution contained about 10 mM potassium ferricyanide ($K_3[Fe(CN)_6]$), which was prepared in Tris–HCl buffer (0.05 M) with the pH adjusted to 7.26. To enhance the ionic conductivity of the solution, 1 M KCl was added as a supporting electrolyte.

Ce_2S_3 NPs were added to the electrolyte solution at concentrations of 0 to 80 µM. Tris-HCl buffer served as a reference electrolyte. Voltammetric curves were recorded in the potential window range of -1.0 to +1.0 V at a fixed scan rate of 20 mV s^{-1}. To evaluate the effect of scan rate, it was varied between the scan rate from 10 to 80 mV s^{-1}, while maintaining all other parameters constant. The peak current and peak potential were analyzed to elucidate the electrochemical behaviour, as described previously [12].

2.5.5 Genotoxicity assessment of Ce_2S_3 NPs

The comet assay was performed as previously reported protocol with minor modifications [28]. Fresh human peripheral blood sample (3 mL) was collected in EDTA-coated vials and gently agitated using a gyratory shaker. The hematological status of the blood sample was verified using a three-part differential hematology analyzer. Subsequently, a mixture containing 1 mL of blood and 1 mL of 2% fetal bovine serum (FBS) prepared in phosphate-

buffered saline (PBS) and carefully layered over 1.5 mL of Ficoll-Paque Plus. The resulting sample was centrifuged at 500 rpm for 30 min at room temperature. The lymphocyte-rich buffy coat layer was carefully collected, washed twice with PBS, and resuspended in Roswell Park Memorial Institute (RPMI)-1640 medium supplemented with 10% FBS and 1% antibiotic solution. The cells were incubated at 37 °C for 1 hour, followed by treatment with Ce_2S_3 NPs at concentrations of 500 and 1000 µg mL^{-1} for 4 hours in a 5% CO_2 incubator [29]. Untreated cells were maintained as the negative control, while UV exposed cells were used as the positive control. After treatment, microscope slides were coated with 1% normal melting point agarose (NMPA) and allowed to dry. The cell suspension was then combined with 0.5% low melting point agarose (LMPA), spread onto the precoated slides, and left to solidify at 4 °C. The slides were lysed overnight and electrophoresed under alkaline conditions (0.74 V cm^{-1}, 300 mA for 30 min). After completion of the electrophoresis, the slides were neutralized, stained with ethidium bromide (EtBr), and viewed under a fluorescence microscope at 200X magnification, equipped with an excitation filter of 515–560nm [30]. The DNA damage parameters were calculated using TriTek CometScore software (version 2.9.9.3.8).

3 Results and Discussions

3.1 *Characterization of Ce_2S_3 NPs*

3.1.1 X-ray diffraction and fourier infrared spectroscopic analysis

XRD was utilized to determine the crystal structure and phase composition of Ce_2S_3 NPs. The Bragg reflections observed in the XRD pattern Figure 1(a) confirm the formation of orthorhombic Ce_2S_3. The diffraction pattern exhibits characteristic peaks at 2θ = 16.15°, 23.54°, 25.13°, 26.96°, 33.68°, 41.35°, 42.37°, 43.69°, 45.76°, 49.59°, 50.57°, and 54.86°, which are indexed to the (102), (200), (111), (112), (006), (107), (304), (020), (121), (024), (221), and (316) crystallographic planes, respectively, in good agreement with the standard reference data (PDF No. 04-004-6728). The Ce_2S_3 NPs exhibit high crystallinity, with sharp and well-defined diffraction peaks. Moreover, the absence of secondary-phase or impurity-related diffraction peaks confirms the phase purity of the synthesized material. The average crystallite size of the Ce_2S_3 NPs was estimated using the Debye–Scherrer equation, $D = k\lambda/\beta\cos\theta$ [31]. The calculated average crystallite size is found to be ~46 nm, which confirms the formation of Ce_2S_3 in the nanocrystalline regime.

FTIR spectra of Ce_2S_3 NPs were measured over the range of 400-4000 cm^{-1} as represented in Figure 1(b). The broad and intense absorption feature observed near 3600 cm^{-1} is associated with the O- H stretching mode of hydroxyl groups present due to adsorbed water molecules on the sample. The weak band at 1646 cm^{-1} is attributed to the H-O-H bending vibration of adsorbed water. A band observed at 1387 cm^{-1} can be assigned to the symmetric stretching vibration of nitrate (NO_3^-) groups arising from residual precursor salts on the nanoparticle surface. The numerous peaks observed in the low-wavenumber region below 700 cm^{-1} are characteristic of metal-sulfur bonding. The prominent absorption bands appearing around ~660 cm^{-1} are attributed to the Ce-S stretching vibrations, confirming the formation of Ce_2S_3 nanoparticles [32].

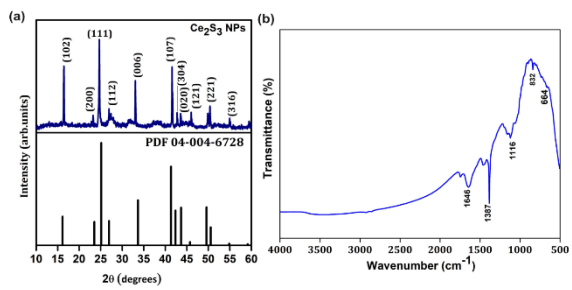


Figure 1: (a) X-ray diffraction pattern and (b) FTIR spectrum of Ce_2S_3 NPs

3.1.2 FE-SEM and TEM analysis

To evaluate the surface morphology of Ce_2S_3 NPs, field-emission SEM analysis was performed, providing insights into their shape, size, and uniformity [33]. As depicted in Figure 2 (a-c), the FE-SEM images reveal predominantly near-spherical Ce_2S_3 NPs that form densely packed agglomerated clusters, likely due to their high surface energy and strong interparticle interactions. Ce_2S_3 NPs exhibited particle sizes in the range of approximately 20-40 nm, which is considered suitable for facilitating cellular uptake and molecular interactions. Further analysis of

Applied Science and Engineering Progress, Vol. 20, No. 4, 2027, 8320

Ce_2S_3 NPs showed well-defined uniformity in both size and morphology.

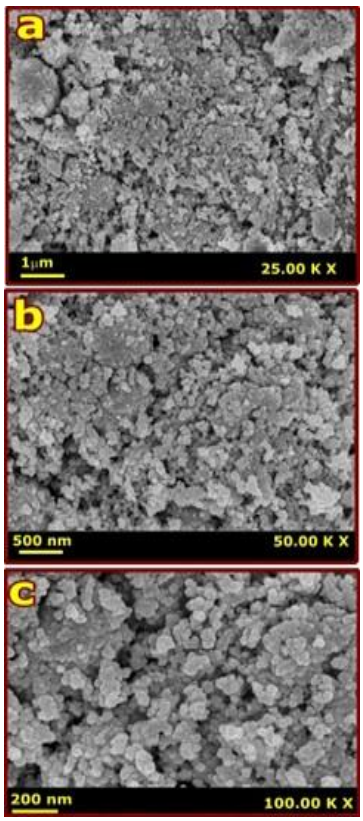


Figure 2: SEM images of Ce_2S_3 NPs with different magnification of (a) 25 KX (b) 50 KX and (c) 100 KX.

The crystal structure and microstructural variations of Ce_2S_3 NPs were analyzed by high-resolution transmission electron microscopy (TEM), which confirms the nano size and structural properties of Ce_2S_3 NPs [34]. The TEM images as depicted in Figure 3(a) showed spherical aggregates with the particle sizes varying from approximately 16 to 37 nm, with an estimated average size of about 23 nm Figure 3(b). The SAED pattern Figure 3(c) exhibits a well-defined circular pattern with bright spots confirming the nanocrystalline structure. The HRTEM image Figure 3(d) shows the well-formed lattice fringes, and the d-spacing calculated was found to be 0.330 nm, which can be indexed to the (112) crystallographic plane of orthorhombic Ce_2S_3. The measured interplanar spacing supports the formation of Ce_2S_3 NPs and is in good agreement with the d-spacing values determined from the XRD analysis, thereby confirming the phase purity and orthorhombic crystal structure of the synthesized Ce_2S_3 NPs.

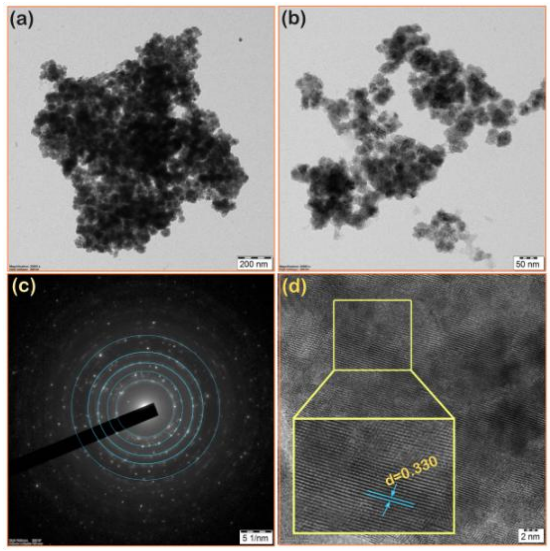


Figure 3: TEM images of Ce_2S_3 NPs. (a,b) TEM images showing nearly spherical aggregates with particle with particle size of approximately 16-37 nm (c) SAED pattern confirming the nanocrystalline nature of Ce_2S_3 NPs (d) HRTEM image showing distinct lattice fringes with d-spacing of 0.330 nm.

3.1.3 Surface charge of Ce_2S_3 NPs

The point of zero charge (pH_pzc) of Ce_2S_3 NPs was determined from the plot of ΔpH (pH_{final}-$pH_{initial}$) as a function of the initial pH. The pH_pzc corresponds to the point where ΔpH equals zero. Figure 4 exhibits a pH_pzc value of 5.2 for Ce_2S_3 NPs. Below this pH, protonation of surface sites leads to a positively charged surface, whereas above the pH_pzc, the surface will become negatively charged due to deprotonation [35], [36]**.** All measurements were performed in 0.01 NaCl to ensure a consistent ionic strength and minimize variations arising from changes in electrolyte concentration. At this low ionic strength, limited charge screening preserves the nanoparticle's intrinsic surface charge, promoting electrostatic interactions with DNA. Whereas higher ionic strength may result in background interference from the electrolyte ions masking the NPs' interaction with DNA.

The pH_pzc is an important parameter for predicting the surface- charge characteristics of Ce_2S_3 NPs, and it influences DNA binding. Because physiological pH (~7.4) is higher than pH_pzc, the

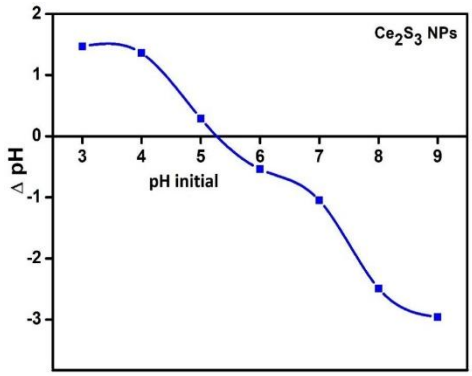


Figure 4: Point zero charge (pHpzc) of Ce_2S_3 NPs.

Ce_2S_3 NPs surface is primarily negatively charged. Nevertheless, stable NP-DNA interactions can still occur via non-electrostatic forces such as hydrogen bonding, van der Waals forces, and surface coordination, and charge shielding by ions in the buffer solution, which collectively reduce electrostatic repulsion and facilitate stable binding between Ce_2S_3 NPs and DNA. Overall, the pH_pzc-derived surface charge behaviour plays an important role in regulating NP-DNA interactions [35].

3.2 *DNA Binding Studies of Ce_2S_3 NPs with CT-DNA*

3.2.1 UV-visible spectroscopy

The interaction behavior between Ce_2S_3 NPs and CT-DNA was examined using UV-visible spectroscopy. DNA-ligand interactions are generally characterized by two spectral characteristics, hypochromism, which shows stabilization of the DNA helix, and hyperchromism, which shows partial disruption of the DNA structure.

The interaction between Ce_2S_3 NPs and CT-DNA was examined by observing UV-visible spectra in the 200-800 nm region with a gradual increase in the CT-DNA concentration at a fixed concentration of NPs [12]. As shown in Figure 5(a), a continuous decrease in absorbance intensity was observed, exhibiting a distinct hypochromic effect. The distinct absorption peak at 328 nm showed decreased intensity without any significant shift in wavelength, indicating a non-intercalative binding mechanism. Instead, the combination of hypochromism and the absence of peak shift shows a non-covalent interaction, which involves electrostatic association or groove binding, which contributes to enhancement of the DNA double helical structure [37].

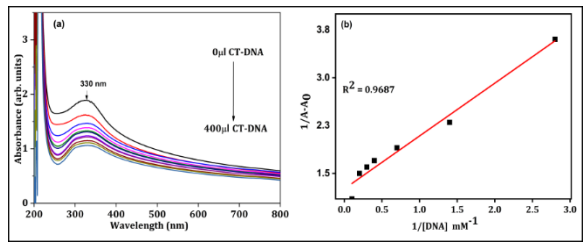


Figure 5: (a) UV-visible absorption spectra of Ce_2S_3 NPs in the presence of increasing concentration of CT-DNA (0 - 400 µl) (b) the linear plot of $1/(A - A_0)$ versus 1/DNA for determination of binding constant.

The binding constant (K_b) for the Ce_2S_3 NP-CT-DNA complex was calculated using a reciprocal plot of $1/(A - A_0)$ versus 1/C, as shown in Figure 5 (b) yielding a value of 5.186×10^4 M^{-1}, which indicates a moderate binding affinity. This magnitude of binding constant is characteristic of non-intercalative interactions and is consistent with the spectroscopic observations.

3.2.2 Fluorescence spectroscopy

The interaction of Ce_2S_3 NPs with CT-DNA was examined using the ethidium bromide displacement assay, as fluorescence emission spectroscopy is a sensitive and selective technique for probing DNA–nanoparticle interactions. The DNA-EtBr complex exhibited a strong fluorescence emission around 600 nm upon excitation at 465 nm. Any process that disrupts or inhibits the intercalative binding of EtBr to DNA results in a decrease in fluorescence intensity [38].

As shown in Figure 6(a), stepwise addition of Ce_2S_3 NPs at concentrations of 50, 100, and 150 µM results in a distinct decrease in fluorescence intensity of the DNA-EtBr complex. This quenching effect shows that EtBr molecules are substituted from the DNA helix by Ce_2S_3 NPs. Notably, the maximum emission shows no significant change, showing that quenching is mainly determined by intensity changes rather than any shift in wavelength. These findings correspond to a non-covalent mode of interaction between Ce_2S_3 NPs and CT-DNA, which arises from surface-mediated interactions and competitive binding processes. The binding constant was further analyzed using the Stern-Volmer equation [39].

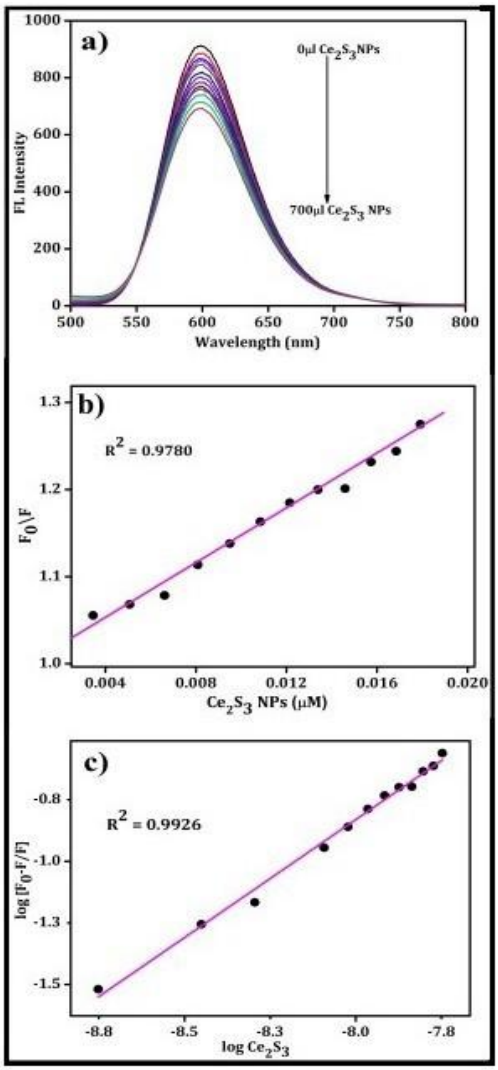


Figure 6: Competitive displacement assays (a) Fluorescence emission spectra of the ethidium bromide-intercalated CT-DNA complex recorded after incubation with increasing concentrations of Ce_2S_3 NPs (0–700 µM). (b) Stern Volmer plot of Ce_2S_3 NPs with CT-DNA interaction. (c) The modified Stern-Volmer plot illustrating the quenching of CT-DNA fluorescence by Ce_2S_3 NPs.

$$F_0/F = 1 + K_{sv}[Ce_2S_3] = 1 + k_q \tau [Ce_2S_3] \quad (1)$$

In this equation, F_0 and F depict fluorescence intensities in the presence and absence of increasing concentrations of Ce_2S_3 NPs, K_{sv} denotes the Stern-Volmer quenching constant, calculated as the slope of the graph of F_0/F versus $[Ce_2S_3]$, as shown in Figure 5(b). The Stern-Volmer quenching constant [40]. (K_{sv}) was found to be $1.573 \times 10^4\ M^{-1}$.

The biomolecule quenching constant K_q was determined by the following equation.

$$K_q = \frac{K_{sv}}{\tau} \quad (2)$$

Here τ denotes the average lifetime of DNA, i.e. 10^{-8} [40], [41]. K_q was found to be 1.573×10^{12}.

Fluorescence quenching mechanisms occur via dynamic quenching and static quenching, the latter arising from ground-state complex formation between fluorophore and quencher. These mechanisms can be identified by comparing the bimolecular quenching constant (K_q) with the diffusion-controlled quenching rate constant in aqueous media, typically ~$2 \times 10^{10}\ M^{-1}\ s^{-1}$. When the calculated Kq value significantly exceeds this diffusion-controlled limit, the quenching process cannot be explained by collisional encounters and instead confirms the successful formation of a non-fluorescent ground-state complex prior to excitation.

In the present study, the obtained K_q value greatly exceeds the diffusion-controlled limit, which demonstrates that fluorescence quenching of the DNA-EtBr complex by Ce_2S_3 NPs is primarily governed by static quenching, which is attributed to the ground-state complex formation [42]. The binding constant (K_b) was determined by the modified Stern-Volmer equation.

$$log\ [(F_0 - F)/F] = log\ K_b + n\ log\ [Ce_2S_3] \quad (3)$$

The graph of Log (F_0-F/F) v/s log (Ce_2S_3 NPs) yields a straight line, where the Y-intercept corresponds to K_b Figure 6c. The value of the binding constant K_b was found to be $6.714 \times 10^6\ M^{-1}$. The fluorescence binding constant was determined using the EtBr displacement assay and double-log equation. Due to its sensitivity to DNA microenvironment changes, fluorescence often gives a higher apparent binding constant compared to UV-Vis spectroscopy that monitors the changes in ground-state electronic absorption. The calculated K_b value was further utilized to estimate the standard free energy change(ΔG°) for binding of Ce_2S_3 NPs to CT- DNA following the equation given below.

$$\Delta G_0 = -2.303\ RT\ (log\ K_b) \quad (4)$$

Here, ΔG^0 denotes the standard free energy change, R - gas constant (1.987 cal mol^{-1} k^{-1}). T - Absolute temperature (298 K) and K_b - binding constant. The value of ΔG^0 is -9.2769 kcal/mol, indicating spontaneous binding between Ce_2S_3 NPs and CT-DNA.

3.2.3 Circular dichroism

CD spectroscopy was implemented to examine conformational changes in CT-DNA upon interaction with Ce_2S_3 NPs. The CD spectra revealed two distinctive characteristic peaks. CT-DNA in its native B-form exhibits two distinct bands: a positive band at 273 nm, which is attributed to the base stacking interactions, and a negative band around 236 nm, associated with polynucleotide helicity [43], [44]. Ce_2S_3 NPs lack intrinsic optical activity; however, induced CD signals arise due to chiral perturbation upon binding to DNA. Upon addition of increasing concentrations of Ce_2S_3 NPs, the CD spectra of CT-DNA exhibited a concentration-dependent decrease in peak intensity of both positive and negative bands without any remarkable shift in the band position. As illustrated in Figure 7, upon the addition of Ce_2S_3 NPs, it can be observed that the changes in ellipticity indicate that the native B-form of DNA remains intact with no major structural changes. These findings rule out the intercalative mode of binding, thereby revealing that Ce_2S_3 NPs bind to the CT-DNA through electrostatic interactions. This interpretation is in agreement with the results obtained from the preceding spectroscopic analysis.

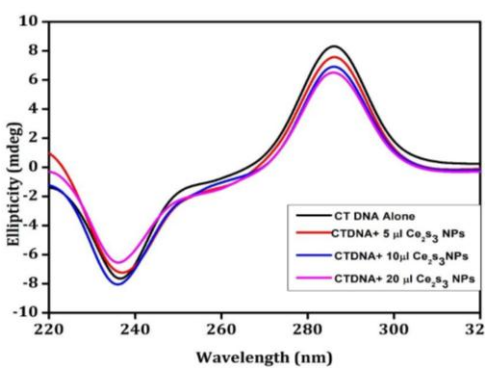


Figure 7: Circular Dichroism spectra of CT-DNA at varying concentrations of Ce_2S_3 NPs (0 – 20 µl).

Furthermore, quantitative analyses have been carried out by calculating the percentage change in ellipticity at the characteristic CD bands (273 and 236 nm). The positive band showed a concentration-dependent decrease in ellipticity (21.9%, 48.5%, and 48.9% for 5, 10, and 20 µL Ce_2S_3 NPs, respectively). Whereas only minor variations were observed in the negative band without any wavelength shift. These results indicate slight perturbation of DNA base stacking while preserving the native B-form conformation, thereby strengthening the conclusion that Ce_2S_3 NPs interact predominantly through electrostatic interactions without causing major structural disruption of DNA.

3.2.4 Cyclic voltammetry

CV is widely employed as an electrochemical method for investigating *in vitro* metal based NPs and DNA interactions, as it effectively mimics many features of biological electron- transfer processes. CV effective technique owing to its high sensitivity, simplicity, and suitability for evaluating the kinetic and thermodynamic properties of the synthesized NPs. The CV information provides valuable insights into the redox nature of a compound, enabling the investigation of binding interactions of CT-DNA through changes in redox potential and current [45]-[47].

In the experimental setup, cyclic voltammograms were recorded as the concentration of Ce_2S_3 NP was increased from 0 to 80 µM, using $K_3[Fe(CN)_6]$ in a Tris-HCl buffer supplemented with KCl as the analyte. The glassy carbon electrode was coated with CT-DNA, the electrode surface becomes rich in negatively charged phosphate groups, which can interact with the redox-active particles. The addition of the Ce_2S_3 NPs into the electrolyte significantly alters the electrochemical response. The gradual increase in the peak current is observed, which is attributed to the interaction between CT-DNA and Ce_2S_3 NPs, which enhances the electroactive surface area and facilitates electron transfer at the electrode-electrolyte interface Figure 8(a).

The peak potentials shift towards lower potentials (from 0.281v at 0 Ce_2S_3 NPs to 0.268 V at 20 Ce_2S_3 NPs), which suggests that, due to the improved electrode interface, the redox reactions become more favorable. The relatively stable current response across the cycles, without the drastic distortion of the CV shape, indicates good electrochemical stability and stable quasi-reversible redox behavior. The interaction between Ce_2S_3 NPs to CT-DNA modified electrode is

mainly attributed to the electrostatic interactions between the DNA phosphate backbone, which carries a negative charge, and positively charged regions on the Ce_2S_3 NPs surface, complemented by possible coordination interactions with Ce^{3+} centres. These electrostatic interactions promote the stable NPs immobilization at the DNA layer, thereby increasing the electroactive surface area and facilitating electron transfer.

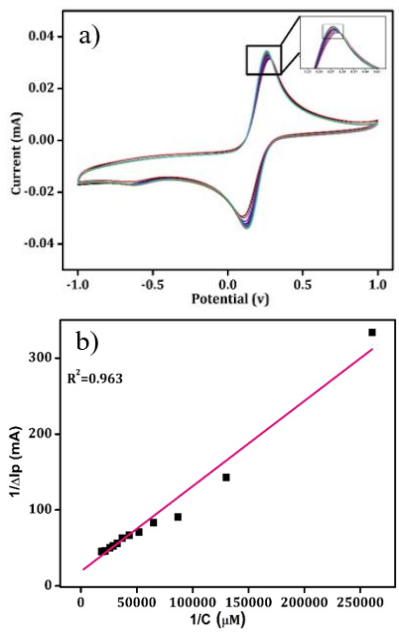


Figure 8 : (a) Cyclic voltammograms of CT-DNA-modified electrodes in the presence of Ce_2S_3 NPs (0–80 μM). (b) Plot of inverse current decrease versus reciprocal Ce_2S_3 NP concentration.

To further evaluate the electrochemical response, the linear relationship between the reciprocal of the peak current ($1/I_p$) and the reciprocal of the Ce_2S_3 NP concentration (1/C) was examined Figure 8(b). The plot exhibited a strong linear correlation, with an R^2 value of 0.963, indicating the high sensitivity of the electrode toward variations in Ce_2S_3 NP concentration. This result demonstrates the reliable analytical response of the electrode system and its potential applicability for the electrochemical detection of Ce_2S_3 NPs under repeated cycling conditions. Based on the redox peak current values, the binding constant was determined via the Langmuir equation [12], [43]

$$1/\Delta Ip = 1/\Delta I_{pmax} + 1/\Delta I_{pmax} K_a \, C \qquad (5)$$

Here, ΔIp represents the current drop, ΔIp_{max} denotes the maximum decrease in current, Ka denotes the binding constant between Ce_2S_3 NPs and CT-DNA, and C represents the concentration of Ce_2S_3 NPs. The slope and intercept from the 1/ [Ce_2S_3 NP] vs. 1/ΔIp graph Figure 8(b) were determined and Ka was found to be 1.702×10^4 M^{-1} for Ce_2S_3 NPs. The literature reported that the electrostatic association of a molecule with the negatively charged deoxyribose-phosphate backbone of DNA typically results in negative shifts in the peak potentials [48]. Therefore, it is evident that the negative peak potential shift in the CV behavior is attributed to the Electrostatic interaction.

3.2.5 Effect of scan rate

The interaction between a CT-DNA-modified electrode and Ce_2S_3 NP could be highly influenced by either diffusion or adsorption processes. The electrochemical investigation was done at varying scan rates, which has a crucial role in examining whether the process of binding involves adsorption or diffusion Figure 9(a). When it is a diffusion-controlled process, a linear relationship is observed between peak current and the square root of scan rate. In contrast, for an adsorption-controlled process, the peak current varies linearly with the scan rate itself [12]. The observed linear relationship between the square root of the scan rate and the peak current as observed in Figure 9 (c) indicates that the electrochemical reaction at the DNA-modified glassy carbon electrode (GCE) is primarily governed by a diffusion-controlled process.

3.2.6 Genotoxicity assessment of Ce_2S_3 NPs

The genotoxic potential of Ce_2S_3 NPs in human peripheral blood lymphocytes was investigated by means of the comet assay [49]The DNA damage was evaluated using olive tail moment (OTM), a parameter that combines both DNA migration distance and proportion of DNA in the comet tail. As depicted in Figure 10A, the OTM values and Figure 10B illustrate the corresponding comet images at two different concentrations. The negative control, as depicted in Figure 10B (a), exhibits intact nuclei with negligible tail formation, consistent with the very low OTM (<1) values. The positive control Figure 10B (b) shows prominent DNA migration and long comet tails, consistent with the high OTM (~10) values,

confirming extensive DNA damage. Ce_2S_3 NP treated cells Figure 10B (c) & (d) show a clear concentration-dependent increase in DNA damage, aligned with the trend observed in Figure 10A. 500 µg/mL treated group exhibits moderate tail formation with an OTM of ~1.6, indicating low genotoxicity compared to the positive control. In comparison, the 1000 µg/mL treatment results in visibly longer tails and a higher OTM (~3.8), indicating significantly increased DNA damage relative to both the negative control and lower concentrations. The observations demonstrate that Ce_2S_3 NPs induce genotoxic stress in a dose-dependent manner, with higher concentrations.

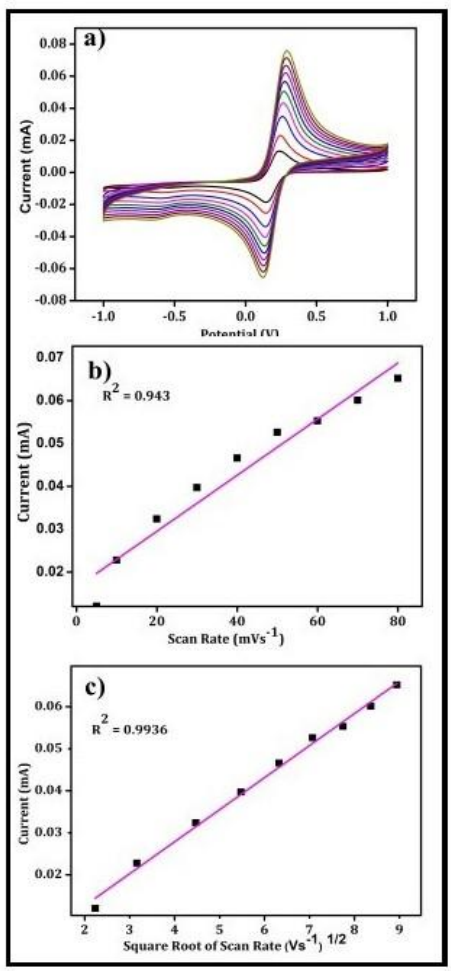


Figure 9: (a) Effect of scan rate on the CV response of the CT-DNA-modified GCE in the presence of Ce_2S_3 NPs. (b) Peak current versus scan rate. (c) Peak current versus square root of scan rate.

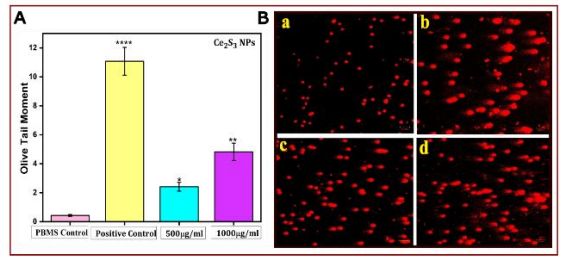


Figure 10: Genotoxicity effects of Ce_2S_3 NPs in human peripheral blood mononuclear cells, evaluated via comet assay (A) Olive Tail Moment (OTM) following exposure to 500 and 1000 µg/mL Ce_2S_3 NPs. Data are expressed as mean ± SD (n = 3). Statistical significance was determined by one-way ANOVA followed by Tukey's multiple comparison test (*p-value < 0.05, **p-value < 0.01, ****p-value < 0.0001 vs. untreated PBMC control). (B) Representative comet images of (a) untreated PBMC control, (b) positive control, (c) 500 µg/mL Ce_2S_3 NPs, and (d) 1000 µg/mL Ce_2S_3 NPs.

4 Conclusions

Ce_2S_3 NPs were successfully synthesized via a solvothermal route and characterized using XRD, FTIR, FE-SEM, and TEM, confirming an orthorhombic crystalline structure, Ce–S bond formation, and nearly spherical morphology with particle sizes of 16-40 nm. Surface charge analysis revealed a point of zero charge (pH_pzc) of 5.2, indicating pH-dependent protonation–deprotonation behavior relevant to biomolecular interactions. The interaction between Ce_2S_3 NPs and calf thymus DNA (CT-DNA) was comprehensively investigated using UV-visible absorption, fluorescence spectroscopy, circular dichroism, and cyclic voltammetry. Spectroscopic studies demonstrated spontaneous and stable DNA binding dominated by noncovalent interactions, primarily electrostatic in nature, with possible minor contributions from surface adsorption or partial intercalation. The calculated binding constants and negative Gibbs free energy values confirmed the thermodynamically favorable nature of the interaction. Electrochemical investigations further supported a diffusion-controlled binding process and revealed stable quasi-reversible redox behavior at the DNA-modified electrode interface.

Genotoxicity assessment using the comet assay revealed a clear dose-dependent increase in DNA damage upon exposure to Ce_2S_3 NPs. While lower

nanoparticle concentrations produced minimal genotoxic effects, higher concentrations resulted in significant DNA strand damage. These findings suggest that direct nanoparticle-DNA interactions at elevated doses may contribute to genotoxicity, potentially through DNA conformational perturbation and/or nanoparticle-induced oxidative stress. Overall, this study highlights the importance of concentration control and surface engineering strategies to minimize genotoxic effects and supports the cautious development of Ce_2S_3 NPs for potential biomedical and bioanalytical applications.

Acknowledgments

S. Farhat Afsar is grateful to the Management, Principal and HOD of Biotechnology and Chemistry of M.S. Ramaiah Institute of Technology, Bangalore, for their constant support and encouragement. Farhat Afsar is grateful to Indians Institute of Science, Bangalore, for helping to perform Circular Dichroism.

Author Contributions

All authors contributed to the study conception and design. Material preparation, data collection and analysis were performed by Farhat Afsar, D. L. Monika, R. Hari Krishna, and M N Chandraprabha. The first draft of the manuscript was written by Farhat Afsar, and all authors commented on previous versions of the manuscript. Conceptualization, Project Guidance and supervision of the work were done by Dr. M N Chandraprabha and Dr. R. Hari Krishna. All authors read and approved the final manuscript.

Data Availability:

The datasets generated during and/or analysed during the current study are available from the corresponding author on reasonable request.

Conflicts of Interest

The authors declare no conflict of interest.

Funding

The authors declare that no funds, grants, or other support were received during the preparation of this manuscript.

Competing Interests

The authors have no relevant financial or non-financial interests to disclose.

Declaration of generative AI and AI-assisted technologies in the writing process

The authors utilized the ChatGPT tool to enhance the language and readability of the manuscript.

References

[1] V. Ramalingam, S. Raja, S. Sundaramahalingam, and R. Rajaram, "Chemical fabrication of graphene oxide nanosheets attenuates biofilm formation of human clinical pathogens," *Bioorganic Chemistry*, vol. 83, pp. 326–335, Mar. 2019, doi: 10.1016/j.bioorg.2018.10.052.

[2] L. L. Tayo, "Stimuli-responsive nanocarriers for intracellular delivery," *Biophysical Reviews*, vol. 9, no. 6, pp. 931–940, Nov. 2017, doi: 10.1007/s12551-017-0341-z.

[3] S. Islam et al., "Nanomaterials: applications in biomedicine and biotechnology," *in Handbook of Nanomaterials and Nanocomposites for Energy and Environmental Applications*, Cham: Springer, pp. 1–18, Aug. 2020, doi: 10.1007/978-3-030-11155-7_4-1.

[4] H. Verma, M. Aggarwal, and S. Kumar, "Opportunities and significance of nanoparticle–DNA binding in medical biotechnology: a review," *Cureus*, vol. 14, no. 11, Nov. 2022, Art. no. e31005, doi: 10.7759/cureus.31005.

[5] S. Anjum et al., "Emerging applications of nanotechnology in healthcare systems: grand challenges and perspectives," *Pharmaceuticals*, vol. 14, no. 8, Jul. 2021, Art. no. 707, doi: 10.3390/ph14080707.

[6] U. Singh et al., "DNA-functionalized nanoparticles for targeted biosensing and biological applications," *ACS Omega*, vol. 5, no. 48, pp. 30767–30774, Nov. 2020, doi: 10.1021/acsomega.0c03656.

[7] M. Sirajuddin, S. Ali, and A. Badshah, "Drug–DNA interactions and their study by UV–Visible, fluorescence spectroscopies and

cyclic voltametry," *Journal of Photochemistry and Photobiology B: Biology*, vol. 124, pp. 1–19, Jul. 2013, doi: 10.1016/j.jphotobiol.2013.03.013.

[8] S. U. Rehman, T. Sarwar, M. A. Husain, H. M. Ishqi, and M. Tabish, "Studying non-covalent drug–DNA interactions," *Archives of Biochemistry and Biophysics*, vol. 576, pp. 49–60, Jun. 2015, doi: 10.1016/j.abb.2015.03.024.

[9] X.-L. Li, Y.-J. Hu, H. Wang, B.-Q. Yu, and H.-L. Yue, "Molecular spectroscopy evidence of berberine binding to DNA: comparative binding and thermodynamic profile of intercalation," *Biomacromolecules*, vol. 13, no. 3, pp. 873–880, Feb. 2012, doi: 10.1021/bm2017959.

[10] M. Saeed et al., "Comprehensive reviews on the potential applications of inorganic metal sulfide nanostructures in biological, environmental, healthcare, and energy generation and storage," *Reviews in Inorganic Chemistry*, vol. 45, no. 2, pp. 237–274, May 2024, doi: 10.1515/revic-2024-0016.

[11] W. Fei et al., "Engineering of bioactive metal sulfide nanomaterials for cancer therapy," *Journal of Nanobiotechnology*, vol. 19, no. 1, Mar. 2021, Art. no. 93, doi: 10.1186/s12951-021-00839-y.

[12] M. Mahanthappa, M. A. Savanur, and S. Yellappa, "Molecular interaction studies of zinc sulphide nanoparticles with DNA and its consequence: a multitechnique approach," *Luminescence*, vol. 36, no. 1, pp. 45–56, Jul. 2020, doi: 10.1002/bio.3912.

[13] H. Kumar et al., "Antioxidant functionalized nanoparticles: a combat against oxidative stress," *Nanomaterials*, vol. 10, no. 7, Jul. 2020, Art. no. 1334, doi: 10.3390/nano10071334.

[14] A. Shetty, H. Lang, and S. Chandra, "Metal sulfide nanoparticles for imaging and phototherapeutic applications," *Molecules*, vol. 28, no. 6, Mar. 2023, Art. no. 2553, doi: 10.3390/molecules28062553.

[15] S. Das, J. M. Dowding, K. E. Klump, J. F. McGinnis, W. Self, and S. Seal, "Cerium oxide nanoparticles: applications and prospects in nanomedicine," *Nanomedicine*, vol. 8, no. 9, pp. 1483–1508, Aug. 2013, doi: 10.2217/nnm.13.133.

[16] S. A. Abdulsattar, "Cerium oxide nanoparticles role as antioxidant," *Medical Journal of Babylon*, vol. 21, no. 2, pp. 235–239, Jul. 2024, doi: 10.4103/MJBL.MJBL_1022_23.

[17] Y. Wu and H. T. Ta, "Different approaches to synthesising cerium oxide nanoparticles and their corresponding physical characteristics, and ROS scavenging and anti-inflammatory capabilities," *Journal of Materials Chemistry B*, vol. 9, no. 36, pp. 7291–7301, Jul. 2021, doi: 10.1039/d1tb01091c.

[18] A. L. Chibac-Scutaru, V. Podasca, I. A. Dascalu, and V. Melinte, "Exploring the influence of synthesis parameters on the optical properties for various CeO_2 NPs," *Nanomaterials*, vol. 12, no. 9, Apr. 2022, Art no. 1402, doi: 10.3390/nano12091402.

[19] R. Liman, Y. Acikbas, and İ. H. Ciğerci, "Cytotoxicity and genotoxicity of cerium oxide micro and nanoparticles by Allium and Comet tests," *Ecotoxicology and Environmental Safety*, vol. 168, pp. 408–414, Jan. 2019, doi: 10.1016/j.ecoenv.2018.10.088.

[20] C. Sambathkumar, N. Nallamuthu, M. K. Kumar, S. Sudhahar, and P. Devendran, "Electrochemical exploration of cobalt sulfide nanoparticles synthesis using cobalt diethyldithiocarbamate as single source precursor for hybrid supercapacitor device," *Journal of Alloys and Compounds*, vol. 920, Nov. 2022, Art. no. 165839, doi: 10.1016/j.jallcom.2022.165839.

[21] Q. Wang, S.-R. Zhang, and X. Ji, "Investigation of interaction of antibacterial drug sulfamethoxazole with human serum albumin by molecular modeling and multi-spectroscopic method," *Spectrochimica Acta Part A: Molecular and Biomolecular Spectroscopy*, vol. 124, pp. 84–90, Apr. 2014, doi: 10.1016/j.saa.2013.12.100.

[22] G. Lucena-Aguilar, A. M. Sánchez-López, C. Barberán-Aceituno, J. A. Carrillo-Ávila, J. A. López-Guerrero, and R. Aguilar-Quesada, "DNA source selection for downstream applications based on DNA quality indicators analysis," *Biopreservation and Biobanking*,

vol. 14, no. 4, pp. 264–270, May 2016, doi: 10.1089/bio.2015.0064.

[23] A. Yadav, N. Bagotia, S. Yadav, A. K. Sharma, and S. Kumar, "Adsorptive studies on the removal of dyes from single and binary systems using Saccharum munja plant-based novel functionalized CNT composites," *Environmental Technology & Innovation*, vol. 24, Nov. 2021, Art. no. 102015, doi: 10.1016/j.eti.2021.102015.

[24] S. Dan, A. Chattree, J. Naskar, and S. Kamsonlian, "Comparative study of ferromagnetic behaviour in bare and DDMAB-PMMA-PEG modified Manganese Ferrite ($MnFe_2O_4$) nanoparticles," *Materials Today: Proceedings*, vol. 78, pp. 62–68, 2023, doi: 10.1016/j.matpr.2022.11.197.

[25] M. A. Husain, H. M. Ishqi, T. Sarwar, S. U. Rehman, and M. Tabish, "Interaction of indomethacin with calf thymus DNA: a multi-spectroscopic, thermodynamic and molecular modelling approach," *Medchemcomm*, vol. 8, no. 6, pp. 1283–1296, Apr. 2017, doi: 10.1039/c7md00094d.

[26] L. Momeni, B. Shareghi, A. A. Saboury, and S. Farhadian, "Comparative studies on the interaction of spermidine with bovine trypsin by multispectroscopic and docking methods," *The Journal of Physical Chemistry B*, vol. 120, no. 36, pp. 9632–9641, Sep. 2016, doi: 10.1021/acs.jpcb.6b06648.

[27] N. Yadav, A. Singh, and M. Kaushik, "Synthesis and characterization of hydrothermally synthesized superparamagnetic APTS–$ZnFe_2O_4$ nanoparticles: DNA binding studies for exploring biomedical applications," *Chemical Papers*, vol. 74, pp. 1177–1188, Oct. 2019, doi: 10.1007/s11696-019-00953-0.

[28] S. Nandhakumar, S. Parasuraman, M. M. Shanmugam, K. R. Rao, P. Chand, and B. V. Bhat, "Evaluation of DNA damage using single-cell gel electrophoresis (Comet Assay)," *Journal of Pharmacology and Pharmacotherapeutics*, vol. 2, no. 2, pp. 107–111, Jun. 2011, doi: 10.4103/0976-500X.81903.

[29] P. Velumani, N. Palani, A. A. Casmie, R. Senthilvel, and V. Parthasarthy, "Cellular and chromosomal interaction of bio-synthesized copper oxide nanoparticles - Induced nano-cytotoxicity and genotoxicity," *Toxicology in Vitro*, vol. 104, Apr. 2025, Art. no. 106000, doi: 10.1016/j.tiv.2024.106000.

[30] M. Javed, I. Ahmad, A. Ahmad, N. Usmani, and M. Ahmad, "Studies on the alterations in haematological indices, micronuclei induction and pathological marker enzyme activities in Channa punctatus (spotted snakehead) perciformes, channidae exposed to thermal power plant effluent," *SpringerPlus*, vol. 5, no. 1, Jun. 2016, Art. no. 761, doi: 10.1186/s40064-016-2478-9.

[31] A. Singh, Neelam, and M. Kaushik, "Physicochemical investigations of zinc oxide nanoparticles synthesized from Azadirachta Indica (Neem) leaf extract and their interaction with Calf-Thymus DNA," *Results in Physics*, vol. 13, Jun. 2019, Art. no. 102168, doi: 10.1016/j.rinp.2019.102168.

[32] M. M. Rahman, J. Ahmed, and A. M. Asiri, "A glassy carbon electrode modified with γ-Ce_2S_3-decorated CNT nanocomposites for uric acid sensor development: a real sample analysis," *RSC Advances*, vol. 7, no. 24, pp. 14649–14659, Mar. 2017, doi: 10.1039/c6ra27414e.

[33] S. K. Sahu, S. Sikdar, M. K. Ghosh, and T. K. Ghorai, "Investigation of photocatalytic and DNA interaction of novel heterostructured GO/Bi_2O_3/ZnO nanocomposite," *Materials Science for Energy Technologies*, vol. 5, pp. 324–333, 2022, doi: 10.1016/j.mset.2022.07.002.

[34] P. Mohanasundaram and M. Saral A., "Binding properties and biological applications of green synthesized ZnO nanoparticles from neem flower," *Scientific Reports*, vol. 15, no. 1, May 2025, Art. no. 17727, doi: 10.1038/s41598-025-02157-x.

[35] H. N. Umh and Y. Kim, "Sensitivity of nanoparticles' stability at the point of zero charge (PZC)," *Journal of Industrial and Engineering Chemistry*, vol. 20, no. 5, pp. 3175–3178, Sep. 2014, doi: 10.1016/j.jiec.2013.11.062.

[36] C. Benmouhoub, M. Turmine, A. Kadri, and A. Pailleret, "Influence of dodecylsulfate adsorption on the stability of cerium oxide nanoparticle-based colloidal aqueous

dispersions," *Langmuir*, vol. 36, no. 48, pp. 14563–14572, Nov. 2020, doi: 10.1021/acs.langmuir.0c02317.

[37] S. Das, S. Chatterjee, S. Pramanik, P. S. Devi, and G. S. Kumar, "A new insight into the interaction of ZnO with calf thymus DNA through surface defects," *Journal of Photochemistry and Photobiology B: Biology*, vol. 178, pp. 339–347, Jan. 2018, doi: 10.1016/j.jphotobiol.2017.10.039.

[38] L. A. Tavadyan et al., "Exploring the interaction of ethidium bromide and HOECHST 33258 with DNA by means of electrochemical approach," *Biophysical Reviews and Letters*, vol. 12, no. 3, pp. 151–161, Aug. 2017, doi: 10.1142/S1793048017500084.

[39] Í. P. Caruso, W. Vilegas, L. C. de Oliveira, and M. L. Cornélio, "Fluorescence spectroscopic and dynamics simulation studies on isoorientin binding with human serum albumin," *Spectrochimica Acta Part A: Molecular and Biomolecular Spectroscopy*, vol. 228, Mar. 2020, Art. no. 117738, doi: 10.1016/j.saa.2019.117738.

[40] S. Patel, P. Patel, and S. R. Bakshi, "Titanium dioxide nanoparticles: an in vitro study of DNA binding, chromosome aberration assay, and comet assay," *Cytotechnology*, vol. 69, no. 2, pp. 245–263, Jan. 2017, doi: 10.1007/s10616-016-0054-3.

[41] N. Shehata, E. Samir, and I. Kandas, "Gold/QDs-Embedded-Ceria nanoparticles: optical fluorescence enhancement as a quenching sensor," *Applied Sciences*, vol. 10, no. 4, Feb. 2020, Art. no. 1236, doi: 10.3390/app10041236.

[42] E. P. Babu et al., "Extracellularly synthesized ZnO nanoparticles interact with DNA and augment gamma radiation induced DNA damage through reactive oxygen species," *RSC Advances*, vol. 5, no. 76, pp. 62067–62077, Jul. 2015, doi: 10.1039/c5ra09935h.

[43] S. Huang, F. Zhu, Q. Xiao, Y. Liang, Q. Zhou, and W. Su, "Thermodynamic investigation of the interaction between the [(η ^{6} -p-cymene)Ru(benzaldehyde-N ^{4} -phenylthiosemicarbazone)Cl]Cl anticancer drug and ctDNA: multispectroscopic and electrochemical studies," *RSC Advances*, vol. 5, no. 53, pp. 42889–42902, 2015, doi: 10.1039/c5ra03979g.

[44] P. J. Villanueva et al., "Pyronaridine exerts potent cytotoxicity on human breast and hematological cancer cells through induction of apoptosis," *PLoS ONE*, vol. 13, no. 11, Nov. 2018, Art. no. e0206467, doi: 10.1371/journal.pone.0206467.

[45] M. B. Gholivand, H. Peyman, Kh. Gholivand, H. Roshanfekr, A. A. Taherpour, and R. Yaghobi, "Theoretical and instrumental studies of the competitive interaction between aromatic α-Aminobisphosphonates with DNA using binding probes," *Applied Biochemistry and Biotechnology*, vol. 182, no. 3, pp. 925–943, Jan. 2017, doi: 10.1007/s12010-016-2371-6.

[46] N. Arshad and S. I. Farooqi, "Cyclic voltammetric DNA binding investigations on some anticancer potential metal complexes: a review," *Applied Biochemistry and Biotechnology*, vol. 186, no. 4, pp. 1090–1110, Jun. 2018, doi: 10.1007/s12010-018-2818-z.

[47] N. Arshad, M. H. Bhatti, S. I. Farooqi, S. Saleem, and B. Mirza, "Synthesis, photochemical and electrochemical studies on triphenyltin(IV) derivative of (Z)-4-(4-cyanophenylamino)-4-oxobut-2-enoic acid for its binding with DNA: Biological interpretation," *Arabian Journal of Chemistry*, vol. 9, no. 3, pp. 451–462, May 2016, doi: 10.1016/j.arabjc.2014.08.018.

[48] R. Hajian, P. Hossaini, Z. Mehrayin, P. M. Woi, and N. Shams, "DNA-binding studies of valrubicin as a chemotherapy drug using spectroscopy and electrochemical techniques," *Journal of Pharmaceutical Analysis*, vol. 7, no. 3, pp. 176–180, Jun. 2017, doi: 10.1016/j.jpha.2017.01.003.

[49] S. Könen-Adıgüzel and S. Ergene, "In vitro evaluation of the genotoxicity of CeO_2 nanoparticles in human peripheral blood lymphocytes using cytokinesis-block micronucleus test, comet assay, and gamma H2AX," *Toxicology and Industrial Health*, vol. 34, no. 5, pp. 293–300, Mar. 2018, doi: 10.1177/0748233717753780.